

USE OF FIN EQUATION TO CALCULATE NUSSELT NUMBERS FOR ROTATING DISCS

Hui Tang¹, Tony Shardlow² and J Michael Owen¹

¹Department of Mechanical Engineering

²Department of Mathematical Sciences

University of Bath
Bath, BA2 7AY
United Kingdom

ABSTRACT

Conduction in thin discs can be modelled using the fin equation, and there are analytical solutions of this equation for a circular disc with a constant heat-transfer coefficient. However, convection (particularly free convection) in rotating-disc systems is a conjugate problem: the heat transfer in the fluid and the solid are coupled, and the relative effects of conduction and convection are related to the Biot number, Bi , which in turn is related to the Nusselt number. In principle, if the radial distribution of the disc temperature is known then Bi can be determined numerically. But the determination of heat flux from temperature measurements is an example of an inverse problem where small uncertainties in the temperatures can create large uncertainties in the computed heat flux. In this paper, Bayesian statistics are applied to the inverse solution of the circular fin equation to produce reliable estimates of Bi for rotating discs, and numerical experiments using simulated noisy temperature measurements are used to demonstrate the effectiveness of the Bayesian method. Using published experimental temperature measurements, the method is also applied to the conjugate problem of buoyancy-induced flow in the cavity between corotating compressor discs.

NOMENCLATURE

a	inner radius (m)
A	cross-sectional-area of fin (m^2)
b	outer radius (m)
Bi	modified Biot number($= 2hb^2/k_s t$)
Bi_0	Bi number at the MAP point
c, C_1, C_2	constants
C	Matérn covariance matrix
d	fixed vector from numerical fin equation
d_h	hydraulic diameter($= 2(a - r_s)$) (m)
E	coefficient matrix
F	posterior potential
Gr	Grashof number($= (1 - a/b)^3 Re_\phi^2 \beta \Delta T$)
h	heat transfer coefficient (W/m^2K)

I_0, K_0	modified Bessel functions of the first and second kind, order 0
j	index for grid points
J	Jacobian matrix
J_θ	subset of $\{2, \dots, N\}$ to show the position of the temperature measurements
k	thermal conductivity of air (W/mK)
k_s	thermal conductivity of disc (W/mK)
K_q	modified Bessel function of the second kind, order q
l	spatial length scale, parameter for Matérn covariance
L	characteristic length (m)
M	number of temperature measurements
N	number of grid intervals
Nu	Nusselt number ($= hr/k$)
P	probability density function
q	smoothness level, parameter for Matérn covariance
r	radius (m)
r_s	radius of the inner shaft (m)
Ro	Rossby number
Re	Reynolds number
Re_z	axial Reynolds number
Re_ϕ	rotational Reynolds number
s	axial space between discs in cavity (m)
S	fin surface area (m^2)
t	thickness of fin or disc (m)
T	temperature (K)
T_f	temperature of axial throughflow (K)
T_o	temperature of disc (K)
T_{ref}	appropriate reference temperature (K)
V	velocity (m/s)
W	axial component of throughflow velocity (m/s)
x	nondimensional radius ($= r/b$)
β	volume expansion coefficient($= 1/T_{ref}$)(K^{-1})
Γ	gamma function
μ	dynamic viscosity (kg/ms)
ϵ	standard deviation of the experimental data obtained from the Bayesian method

σ	standard deviation, parameter for Matérn covariance
θ	nondimensional temperature for fin (= $(T_o - T_{ref})/(T_b - T_{ref})$)
Θ	nondimensional temperature for experiments (= $(T_o - T_f)/(T_b - T_f)$)
\mathcal{N}	normal distribution
ξ	random error($\sim \mathcal{N}(0,1)$)
ρ	density (kg/m^3)
Ω	angular speed of disc (s^{-1})

Subscripts

a	value at $r = a$
b	value at $r = b$
f	value in axial throughflow
o	value on disc surface
ref	appropriate reference value
z, r, ϕ	axial, radial, circumferential direction

1. INTRODUCTION

Modern high-pressure aeroengine compressors (see Figure 1) present a particular problem for designers: the higher the pressure ratio, the smaller the blades become, and the size of the clearance between the blades and casing has an increasing effect on the compressor performance. To calculate these small clearances for transient and steady conditions, it is necessary to determine the radial growth of the compressor discs. This in turn requires the calculation of the transient temperatures of the

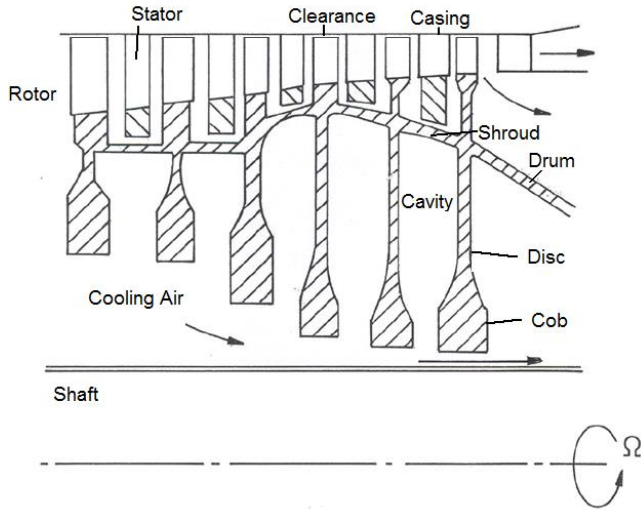


Figure 1 Simplified diagram of high-pressure compressor rotor

discs, which involves the calculation of the values of h , the heat transfer coefficient, for the discs. However, inside the cavity between the corotating compressor discs, the flow is buoyancy-induced. This is an example of a strongly conjugate problem: the

flow in the cavity, and therefore h , depends on the temperature distribution in the discs, and the disc temperature depends on the flow.

Rotating-disc systems can be used to model, theoretically and experimentally, the flow and heat transfer that occurs from turbine and compressor discs in gas-turbine engines. The compressor discs are usually relatively thin - at least over most of their extent - so that the radial temperature differences are much greater than the axial differences. This means that, in principle, the one-dimensional (1D) fin equation (see, for example, Incropera and DeWitt[1]) could be used to determine the heat flux as a function of radius.

The determination of heat flux from temperature measurements is an example of an inverse problem (see, for example, Kaipio and Somersalo[2]). These problems are ill-conditioned, and small uncertainties in the temperature measurements create large uncertainties in the computed heat flux. In recent years, much attention has been focused on inverse problems in heat transfer, and it is now widely accepted that models based on Bayesian statistics can play an important role in their solution. It is the object of this paper to show how these models can be applied to conjugate problems to determine the heat transfer coefficients on rotating discs in general and on compressor discs in particular.

A brief review of Bayesian methods and of buoyancy-induced flow in rotating cavities is given in Section 2, and some analytical and numerical direct solutions of the fin equation are presented in Section 3. Section 4 describes how the Bayesian method can be applied to the inverse solution of the fin equation, and Section 5 applies this method to the computation of Nusselt numbers using simulated and actual temperature measurements on rotating discs. The conclusions are summarised in Section 6, and further details of the Bayesian method are given in the appendix.

2. BRIEF REVIEW OF RELEVANT RESEARCH

2.1 Bayesian method for inverse problems

The interested reader is referred to the monograph of Kaipio and Somersalo[2], which provides an overview of the application of Bayesian statistics to inverse problems in general. For the inverse conduction problem, where measured temperatures are used to compute heat fluxes, Bayesian statistics treat all quantities as random variables, which are modelled in terms of their probability distributions. The ill-posed nature of the inverse problem is overcome by the modelling of the prior distribution (referred to as Bayesian *prior regularisation*) of the unknown heat flux. Statistical inversion then determines the probability distribution, referred to as the *posterior distribution*, of the heat flux after all available information has been incorporated in the model. This posterior distribution provides the heat flux and its confidence intervals.

Kaipio and Fox[3] and Orlande[4] include comprehensive reviews of modern solutions, including Bayesian statistics, of inverse problems in heat transfer, and Wang and Zabaras[5] describe the application of Bayesian models to the inverse conduction problem. Of particular relevance here is the paper by Gnanasekaran and Balaji[6] who applied the Bayesian method to the inverse problem

of natural convection from a vertical fin. They determined the heat transfer coefficients as well as the thermal conductivity of the fin material, and they suggested that only nine thermocouple measurements are needed to produce estimates with reasonable accuracy.

As far as we are aware, Bayesian statistics have not been applied to the inverse problem of heat transfer from rotating discs, and details of the models used in this paper are given in Section 4 and the appendix.

2.2 Buoyancy-induced flow in rotating cavities

A comprehensive review of buoyancy-induced flow and heat transfer in open and closed rotating cavities is given by Owen and Long[7]. The work below relates only to the flow structure for axial-throughflow case, where the Rossby number, Ro , has a significant effect. In addition to the papers referred to below, the books of Childs[7], Owen and Rogers[9] and Tritton[10] provide a theoretical background for a wide range of rotating flows.

As observed by many research workers [e.g. 11, 12], the axial throughflow of air creates a toroidal vortex near the centre of the cavity, as illustrated in Figure 2. The radial extent of the vortex increases as the throughflow increases and as the rotational speed decreases or, more precisely, as Ro increases. At the larger values of Ro , the tangential component of velocity inside the vortex behaves like a free vortex, so that V_ϕ increases as r decreases, and – depending on the value of Ro – vortex breakdown of the central jet can occur. Radially outward of the toroidal vortex, the fluid tends to rotate as a solid body, so that $V_\phi = c\Omega r$; the constant $c = 1$ for isothermal flow, and $c < 1$ when buoyancy-induced flow occurs.

For isothermal flow, unless the non-axisymmetric vortex breakdown occurs, the flow in the cavity is axisymmetric. When the temperature of the discs and shroud is higher than that of the axial throughflow, buoyancy-induced flow can occur and the flow radially outward of the toroidal vortex becomes non-axisymmetric [12]. The asymmetry manifests itself as a pair, or multiple pairs, of cyclonic and anti-cyclonic vortices, which precess about the axis of rotation with an angular velocity less than that of the discs. These vortices create the Coriolis forces necessary for radial outflow to occur in the rotating core of fluid between the boundary layers (usually referred to as Ekman layers) on the rotating discs.

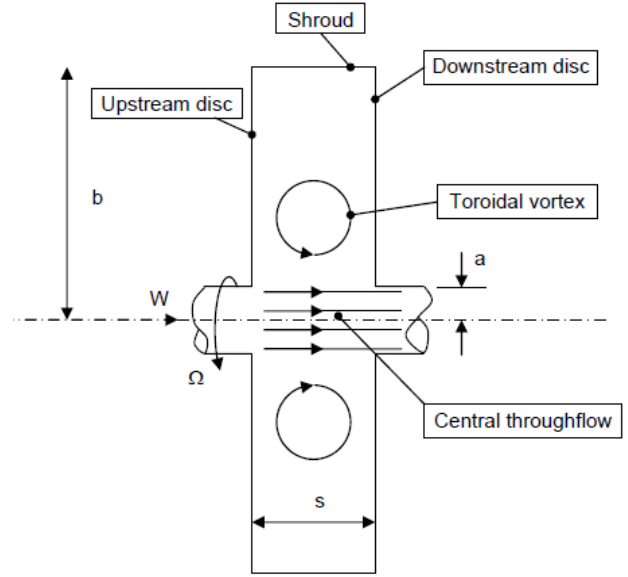


Figure 2 Simplified diagram of axial throughflow in an isothermal rotating cavity

Several research workers have measured the Nusselt numbers on the heated shroud or discs of rotating cavities, using fluxmeters or thermocouples embedded into the surface of the shroud or discs [13-15]. Although Atkins and Kanjirakkad [16] did not determine the Nusselt numbers in their experiments, they did measure the effect of the Rossby, Reynolds and Grashof numbers on the radial distribution of disc temperature; these temperature measurements are used in Section 5 to determine the Nusselt numbers. Their multi-cavity compressor rig is shown in Figure 3, and the flow parameters used in the experiments are given in Table 1 (see Section 5.2).

The shroud (or outer cylindrical surface) could be radiantly heated up to around 410K, and the air temperature at inlet to the cavity was between 297K and 310K. They defined the axial and rotational Reynolds numbers and the Rossby and Grashof numbers as

$$Re_z = 2 \frac{\rho W d_h}{\mu} \quad (1)$$

$$Re_\phi = \frac{\rho \Omega b^2}{\mu} \quad (2)$$

$$Ro = \frac{W}{\Omega a} \quad (3)$$

and

$$Gr = \left(1 - \frac{a}{b}\right)^3 Re_\phi^2 \beta \Delta T \quad (4)$$

where

$$\Delta T = T_{o,b} - T_{ref} \quad (5)$$

The authors assumed $\beta = 1/T_{ref}$, where T_{ref} was taken to be T_f , the mean temperature of the axial throughflow measured downstream of the cavity. They expressed the disc temperature, T_o , in terms of θ , a normalized temperature defined by

$$\theta = \frac{T_o - T_f}{T_{o,b} - T_f} \quad (6)$$

where $T_{o,b}$ is the value of T_o at $r = b$. They measured the temperatures on both sides of the instrumented disc shown in Figure 3, and the flow parameters for their 19 test cases are given in Table 1. Apart from the ‘cob’ region, for $r/b < 0.44$, most of the disc had a uniform thickness of 8 mm, and there was only a small temperature difference across this thin section.

Figure 4 (which is based on Figure 10b in [16]) shows the radial variation of θ measured at a Rossby number of $Ro \approx 1$. Although the shape of the curves depends on the Grashof number, it is shown below that it is in fact the Biot number, which itself is a strong function of the Grashof number, that determines the shape of these curves.

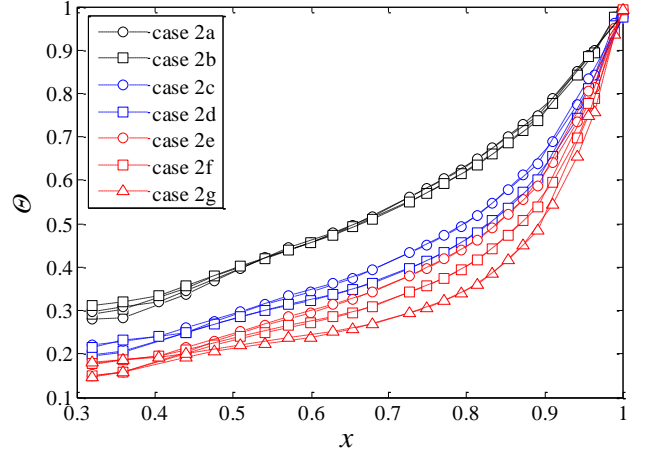


Figure 4 Radial variation of θ , from Atkins and Kanjirakkad [16]

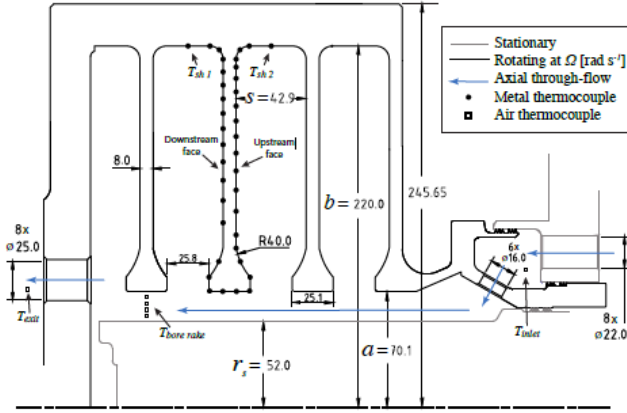


Figure 3 Experimental multi-cavity rig used by Atkins and Kanjirakkad [16] (dimensions in mm).

3. DIRECT SOLUTION OF FIN EQUATION

For the direct problem, the Biot number is specified and the temperature of the fin is calculated.

3.1 Nondimensional version of fin equation

The fin equation (the derivation of which can be found in most text books on heat transfer, such as Incropera and DeWitt [1]) can be expressed as

$$\frac{d}{dr} \left(k_s A \frac{dT_o}{dr} \right) - h(T_o - T_{ref}) \frac{dS}{dr} = 0 \quad (7)$$

where A and S are the cross-sectional and surface areas respectively. For an annular fin of thickness t and inner and outer radii a and b ,

$$A = 2\pi r t \quad (8)$$

$$S = 2\pi(r^2 - a^2) \quad (9)$$

(Note: the fin is cooled symmetrically from both sides, and T_{ref} is a reference temperature. Also, a is used here as the inner radius of the fin and not, as shown in Figure 3, the inner radius of the cavity.)

The fin equation can be expressed in nondimensional terms as

$$\frac{d^2\theta}{dx^2} + \frac{1}{x} \frac{d\theta}{dx} - Bi \theta = 0 \quad (10)$$

where θ is a nondimensional temperature, Bi is a modified Biot number and x is a radius ratio defined by

$$\theta = \frac{T_o - T_{ref}}{T_{o,b} - T_{ref}} \quad (11)$$

$$Bi = 2 \frac{b^2 ht}{t^2 k_s} \quad (12)$$

and

$$x = \frac{r}{b} \quad (13)$$

3.2 Analytical solutions

Eq. (10) is a modified form of Bessel's equation. For constant Biot numbers, the general solution is

$$\theta = C_1 I_0(Bi^{1/2}x) + C_2 K_0(Bi^{1/2}x) \quad (14)$$

Where C_1 and C_2 are constants and I_0 and K_0 are modified Bessel functions of the first and second kind with 0 order. For the case where $\theta = \theta_a$ at $x = x_a = a/b$ and $\theta = \theta_b$ at $x = x_b = 1$, it follows that

$$C_1 = \frac{K_0(Bi^{1/2}x_a)\theta_a - K_0(Bi^{1/2}x_b)\theta_b}{I_0(Bi^{1/2}x_a)K_0(Bi^{1/2}) - I_0(Bi^{1/2})K_0(Bi^{1/2}x_a)} \quad (15)$$

$$C_2 = \frac{I_0(Bi^{1/2}x_a)\theta_b - I_0(Bi^{1/2})\theta_a}{I_0(Bi^{1/2}x_a)K_0(Bi^{1/2}) - I_0(Bi^{1/2})K_0(Bi^{1/2}x_a)} \quad (16)$$

Figure 5 shows the normalised variation of θ v. x according to eq. (14) for a range of Biot numbers with $x_a = 0.3$ for $\theta_a = 0$ and $\theta_b = 1$. The effect of Bi on the shape of θ in Figure 5 is qualitatively similar to the effect of Gr on the shape of θ in Figure 4, although θ in the latter figure was not normalised.

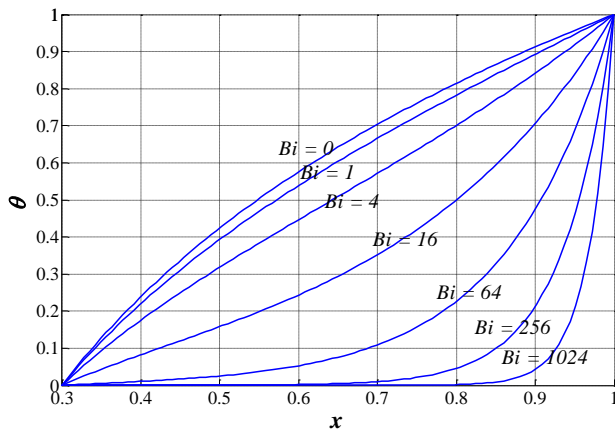


Figure 5 Effect of Bi on theoretical variation of θ v. x for $x_a = 0.3$

3.3 Numerical solution

Numerical solutions are necessary if the Biot number is not constant. Eq. (10) can be approximated by a second-order finite-difference equation. Let x_j for $j = 1, \dots, N + 1$ be a grid of $N + 1$ uniformly spaced grid points between x_a and x_b and let Δx be the constant step length. Then for the j^{th} point on the grid, the temperature θ_j and Bi_j at x_j satisfy

$$\frac{\theta_{j+1} - 2\theta_j + \theta_{j-1}}{\Delta x^2} + \frac{1}{x_j} \frac{\theta_{j+1} - \theta_{j-1}}{2\Delta x} - Bi_j \theta_j = 0, \quad (17)$$

$$(2 \leq j \leq N)$$

The boundary conditions are: $\theta_1 = \theta_a$ at $x = x_a$ and $\theta_b = \theta_{N+1} = 1$ at $x = x_b = 1$. This equation can be directly solved by the tri-diagonal matrix method. The energy balance of the integrated heat fluxes was checked with a relative error less than 2×10^{-4} . With $N = 100$, there was excellent agreement between the numerical and analytical solutions for constant Bi .

4. INVERSE SOLUTION OF FIN EQUATION – BAYESIAN METHOD

The temperature data θ provides information about the Biot numbers via the fin equation. The inverse problem of finding the field of Biot numbers given experimental data θ is ill posed. The problem needs to be regularised by imposing some smoothness conditions on the Biot numbers. To do this, we take a Bayesian approach and give the experimental measurements and the Biot numbers a probabilistic interpretation. Then, Bayes theorem provides a so-called posterior distribution and we can compute the probability distribution for the Biot numbers conditioned on the observation of the temperatures. To extract information from this distribution, we calculate the MAP (*maximum a posteriori*) estimator and 95%-confidence intervals using a Gaussian approximation to the posterior distribution. We work throughout with a discretised set of values for the temperature and Biot numbers. Mathematically, the spatially varying field of Biot numbers is a random field and its probability distribution lives on a function space. To avoid this technicality, we consider only the Biot numbers Bi_j and temperatures θ_j as given by the finite-difference eq. (17).

The reader who is less interested in the theory than in the application of the method might wish to proceed to Section 5.

4.1 Likelihood function

We now introduce the probabilistic model for the data. We assume experimental measurements θ_j are given at a subset of grids points x_j indexed by j from a subset J_θ of $\{2, \dots, N\}$. We further suppose that the observations are noisy and that $\theta_j = \theta_j + \epsilon \xi_j$, where ξ_j are independent $\mathcal{N}(0,1)$ random variables and ϵ^2 is the variance in the experimental data. Then, we can write down the PDF (*probability density function*) of the observations θ given the Biot numbers; this is known as the *likeli-*

hood function. We use the notation $P(\theta|Bi)$ to denote the conditional PDF of θ conditioned on the data Bi . That is, if M is the number of points in J_θ , then

$$P(\theta|Bi) = \frac{1}{(2\pi\epsilon^2)^{\frac{M}{2}}} \exp\left(-\frac{\sum_{j \in J_\theta} (\theta_j - \theta(Bi)_j)^2}{2\epsilon^2}\right) \quad (18)$$

$$= \frac{1}{(2\pi\epsilon^2)^{\frac{M}{2}}} \exp\left(-\frac{(\theta - \theta)^T (\theta - \theta)}{2\epsilon^2}\right)$$

Here, M is the number of data points, θ is an M -vector containing the observations θ_j ($j \in J_\theta$), and θ is a vector of the corresponding θ_j ($j \in J_\theta$) resulting from solving the fin equation with the Biot numbers Bi .

4.2 Prior distribution

The probabilistic interpretation for the Biot numbers is called the prior distribution and expresses realistic assumptions on the field of Biot numbers, such as its smoothness or typical size or the length scale on which it varies. For the prior distribution on Bi , we choose the mean-zero multivariate Gaussian distribution with covariance matrix taken from the Matérn covariance class. The Matérn class of covariance models is used widely in spatial statistics and was introduced by [17,18]. The Matérn class has three parameters: q gives the smoothness or number of derivatives (we take $q = 2$ always), σ^2 gives the variance at each point, and l gives the spatial length scale (for the fin, l is taken to be the total length; for the fin equation, $l = x_b - x_a$) [18]. Then the PDF of the prior distribution is

$$P(Bi) = \frac{1}{(2\pi)^{(N+1)/2} |C|^{1/2}} \exp\left(-\frac{1}{2} Bi^T C^{-1} Bi\right) \quad (19)$$

where $|C|$ denotes the determinant of the matrix C and the covariance matrix C has (i, j) entries

$$C(x_i, x_j) = \frac{\sigma^2}{2^{q-1}\Gamma(q)} \left(\frac{|x_i - x_j|}{l}\right)^q K_q\left(\frac{|x_i - x_j|}{l}\right) \quad (20)$$

Here K_q denotes the modified Bessel function of the second kind of order q and Γ is the gamma function.

The results presented below are sensitive to the choice of q and l . Increasing l or q causes the Biot field to be much stiffer and to have significant variation with a much reduced probability, and it is therefore important to select q and l . To explain the choice of $q = 2$, consider the stiffness or smoothness of the Biot number field modelled like the bending energy in an elastic rod, where second-order derivatives are used. This makes the smoothness parameter $q = 2$ in the Matern covariance a sensible choice, and it means that samples of the Biot-number prior will then have second-order derivatives. (Although it is true that solutions of the fin equation are infinitely differentiable, the Matern distribution models the field of Biot numbers and *not* the temperature distribution.) The choice of

l needs to embody a length scale in the system, and we have chosen this to equal the length of the fin.

4.3 Bayes' theorem

If we assume the Biot number Bi and experimental noise ξ_j are independent, Bayes theorem gives the following expression for the PDF of the posterior distribution

$$P(Bi|\theta) \propto \frac{1}{(2\pi\epsilon^2)^{\frac{M}{2}}} \exp\left(-\frac{(\theta - \theta(Bi))^T (\theta - \theta(Bi))}{2\epsilon^2}\right) \quad (21)$$

$$\times \frac{1}{(2\pi)^{(N+1)/2} |C|^{1/2}} \exp\left(-\frac{1}{2} Bi^T C^{-1} Bi\right)$$

where \propto indicates that we have omitted the constant of proportionality. This PDF can be minimised by the choice of Bi to find the maximum a posteriori (MAP) estimator of the Biot numbers. It is convenient to work with the log of the PDF and determine the MAP estimator by minimising of the so-called posterior potential, F , which is given by

$$F(Bi|\theta) = (M) \ln \epsilon + \frac{(\theta - \theta(Bi))^T (\theta - \theta(Bi))}{2\epsilon^2} \quad (22)$$

$$+ \frac{1}{2} Bi^T C^{-1} Bi$$

The first term depends on data variance only; the second is the data-fitting term; and the third is a smoothing term for the Biot numbers. The last two terms are similar to ones arising from the Tikhonov regularization [2,19]. Further details on the Bayes theorem and the derivation of this formula can be found, for example, in [2].

The MAP estimator is computed by numerical optimisation of the posterior potential $F(Bi|\theta)$ over the choice of Bi , and is adjusted to minimise F . Also, we refine the prior function by reducing σ from a starting value of 1000 until its value is twice the maximum Biot number. (This choice of σ is a compromise between minimising the data variance and reducing the oscillations in Bi .) As shown in Section 5.1, this iterative ad hoc method gives good results for simulated experimental measurements.

To indicate the variability around the MAP estimator, we look for confidence intervals. Rather than do a costly sampling calculation (e.g. Markov chain Monte Carlo sampling methods [20]), we approximate the posterior distribution by a Gaussian distribution using Laplace's method. Essentially, this means we expand the posterior potential $F(Bi|\theta)$ about the MAP estimator and keep only the second-order term. This defines a Gaussian distribution, and confidence intervals are then easily found for the Gaussian approximation. Details of this calculation are given in the appendix. We plot 95%-confidence intervals with the MAP estimator in all experiments discussed below.

5. APPLICATION OF BAYSIAN METHOD TO ROTATING DISCS

5.1 Application using simulated temperature measurements

Alexiou et al. [21], Miché [22] and Günther et al.[23,24] computed the Nusselt numbers on the discs by solving the inverse conduction problem using curve-fits of the experimental temperature measurements on the discs. We now compare this approach, which creates large and unrealistic oscillations in the computed distribution of the Biot number, to the Bayesian method. The examples below use simulated experimental measurements of the disc temperature and a known radial distribution of the Biot number. The distributions of Bi are chosen to be similar to the ones typically found on compressor discs.

First, the true temperature distribution is generated by eq. (17) with $Bi = 100x^5$ and $N = 100$ and with the boundary conditions $x_a = 0.3, \theta_a = \theta_1 = 0.2$ and $x_b = 1, \theta_b = \theta_{N+1} = 1$.

Next, 19 (that is, $M=19$) of the 99 internal data points are selected, and noisy data are generated by adding independent normally-distributed random variables with mean zero and standard deviation equal to 5×10^{-3} . The simulated data are shown in Figure 6a.

Finally, the Bayesian method is applied to the simulated experimental data. The MAP estimator is computed, and ϵ is adjusted to minimise the posterior potential, as described in Section

4.3. The parameters for the Matérn covariance used here were $\sigma = 183, l = 0.7$ and $q = 2$, and the optimum value of ϵ was found to be 4.1×10^{-3} . This value of ϵ is similar to, though a little smaller than, the original standard deviation of 5×10^{-3} . (It is shown in Section 5.2 that the optimum value of ϵ for the experimental data was less than the suggested uncertainty in the measured temperatures.)

Figure 6b shows the Bi results obtained from the inverse solution of eq. (17), and Figure 6a shows the temperature distributions obtained from the direct solution of eq. (17) using these computed values of Bi . Although all the methods give a good approximation to the temperature distribution, only the Bayesian method provides a good estimate of the true Biot numbers. A big advantage of the Bayesian method is that, as shown in the appendix, the confidence intervals can be computed, and it can be seen from Figure 6b that true solution is always within the 95% confidence intervals. (As the uncertainty about the first and second derivatives of θ is greatest at the end points, $x = x_a$ and $x = 1$, the uncertainty in Bi is greatest at these points.)

Figure 7 shows similar results for the case where $Bi = 100x^2$. Having demonstrated the effectiveness of the Bayesian method using simulated experimental data, we now apply the method to actual experimental data.

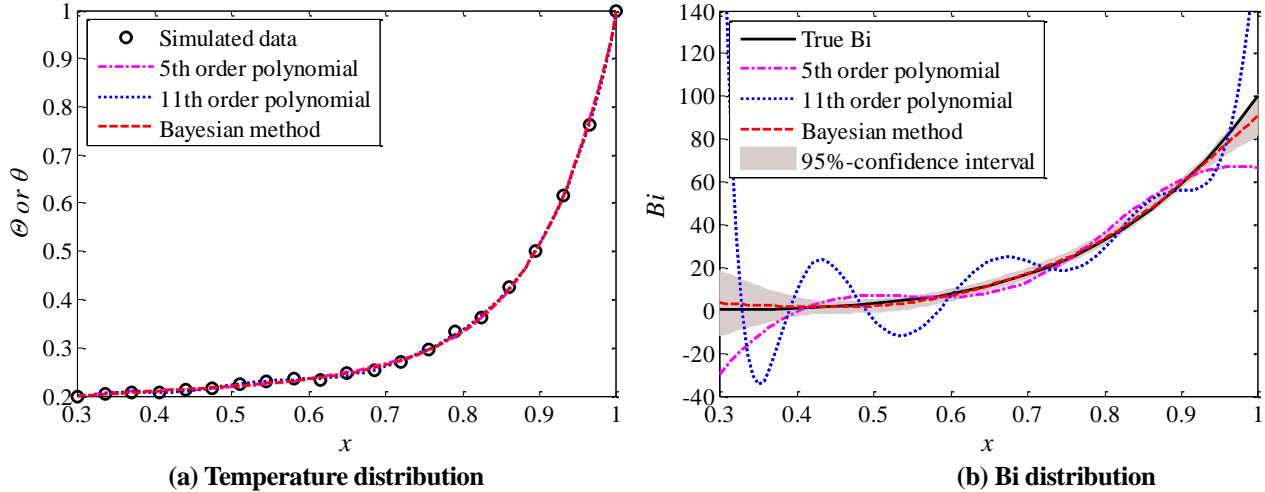


Figure 6 Comparison between Bayesian method and curve-fitting methods for $Bi = 100x^5$

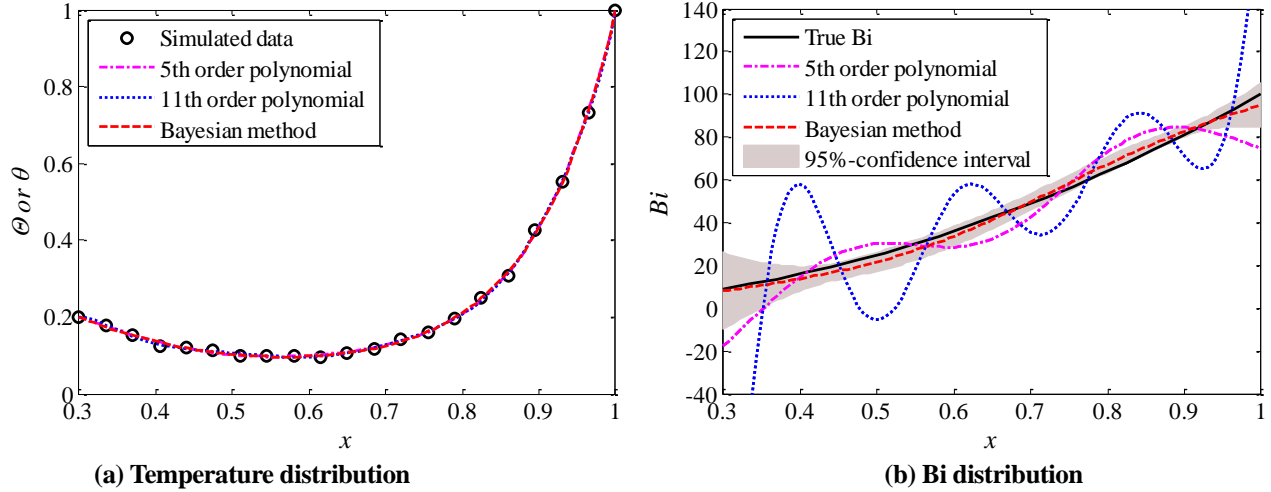


Figure 7 Comparison between Bayesian method and curve-fitting methods for $Bi = 100x^2$

5.2 Application using temperature measurements of Atkins and Kanjirakkad [16].

The experimental temperature measurements used here were obtained by scanning the figures in the paper of Atkins and Kanjirakkad.

For the compressor disc shown in Figure 3, the outer radius was $b = 220$ mm, and for $x > 0.44$ the disc had a uniform thickness of $t = 8$ mm. As the axial temperature differences were small, it was assumed that this outer part of the disc (often referred to as the diaphragm or the web) can be treated as a circular fin. The similarity between the temperature distributions in Figures 4 and 5 gives further support to this assumption.

It should be noted that Bi determined from the fin equation is, in effect, an average value for the two surfaces of the disc. In practice, the different flows in the upstream and downstream cavities could create different values of Bi for the two surfaces. This difference is expected to be greater at the larger values of the Rossby number and the smaller values of x , where the effect of the toroidal vortex is likely to be significant. (In future experiments, if one of the disc surfaces were insulated then this would avoid the average-Biot number problem.)

The average temperatures at $x = x_a = 0.44$ and $x = x_b = 1$ were taken as the boundary conditions of the fin equation, eq. (17), and the 22 temperature measurements ($M = 22$) between these limits were used to determine θ for the Bayesian method. As the measurement points are not uniformly distributed, N is taken to be 300 to achieve more accurate values for $x_j, j \in J_\theta$.

By applying the fin equation and the Bayesian method, the Biot numbers and their confidence intervals were determined in a similar way to that described in Section 5.1 for the simulated experiments. Although the suggested uncertainty in the temperature measurements of Atkins and Kanjirakkad was $\pm 0.5C$ (which – according to the definition of Θ – implies that the uncertainty of Θ was 0.01–0.05), this measure of uncertainty gave poor results. (We suspect this is because the Biot field is smooth and the data is given

multiple spatial locations, which provides information and reduces the uncertainty at a given spatial location. In any case, our method provides a reduced value of ϵ to use in the likelihood function. If the value of ϵ were larger, the resulting posterior distribution would be much less focused around the MAP estimator and would not provide practical results. It can be seen from Table 1 that the optimum values of ϵ obtained from the Bayesian method are much smaller than the suggested uncertainty of Θ .)

For rotating discs, the Nusselt number is usually defined as

$$Nu = \frac{hr}{k} \quad (23a)$$

It follows from the definition of Bi that

$$Nu = \frac{1}{2} \frac{t k_s}{b k} x Bi \quad (23b)$$

The reference temperature, T_{ref} , used in the definition of h for the Biot numbers was taken to be T_f , the temperature of the axial throughflow. For convenience, k_s and k were assumed to be constant, and the thermal conductivity of the titanium disc and the air were taken to be $7.0 \text{ Wm}^{-1}\text{K}^{-1}$ and $0.027 \text{ Wm}^{-1}\text{K}^{-1}$ respectively. It follows that $Nu = 4.71xBi$.

All 19 test cases were analysed, and details of the flow parameters are given in Table 1, in which the tests are arranged in ascending order of Gr . As in Section 5.1, the computed values of Bi obtained from the inverse solution of eq (17) were used to compute θ from the direct solution, and Table 1 shows the values of ϵ obtained in the Bayesian method. (In effect, ϵ is similar to the standard deviation between the computed and measured values of θ .) The table also shows the values of Nu_b , the computed Nusselt number on the disc at $r = b$. Figures 8 to 11, grouped in terms of the approximate Rossby numbers, show the radial distributions of θ and Nu .

Figure 8 shows the results for the six tests at $Ro \approx 5$. For tests 1a and 1b, the Nusselt numbers increase virtually linearly with x .

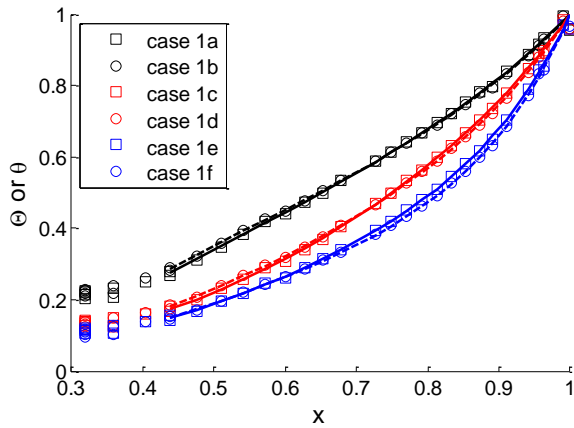
This is consistent with laminar flow over a free disc (see, for example, Owen and Rogers [25]). At these relatively low Grashof and rotational Reynolds numbers ($Gr < 3 \times 10^8$ and $Re_\phi < 7.8 \times 10^4$), it is probable that the effects of buoyancy are very small, and consequently laminar forced-convection dominates for the rotating discs in the cavity. For tests 1c to 1f, the Nusselt numbers for the outer part of the disc ($x > 0.7$) increase sharply as the Grashof number increases, and the data in Table 1 suggest that buoyancy-induced flow starts to dominate in the outer part of the cavity ($x > 0.7$) when $Gr > 8.5 \times 10^8$. In all six tests (and indeed in all the other tests), the computed distributions of temperature are in very good agreement with the measurements.

Figure 9 shows the results for $Ro \approx 1$. All seven tests, where $Gr > 6 \times 10^9$, show evidence of buoyancy-induced flow, and the Nusselt numbers for the outer part of the disc increase monotonically as Gr increases. All distributions of Bi converge to a low value for $x < 0.6$, which suggests that the effects of buoyancy are weak in this region. Similar effects can be seen for the two cases for $Ro \approx 0.6$ in Figure 10.

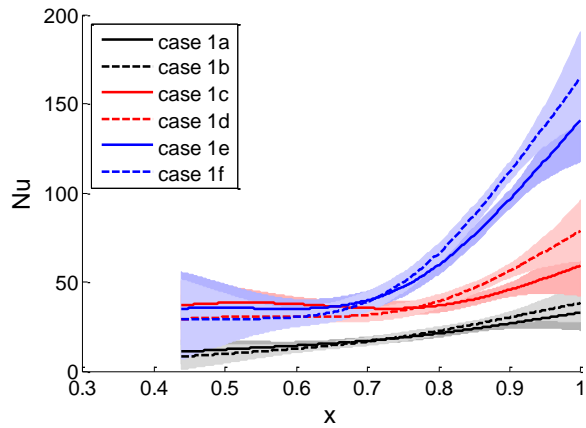
Figure 11, for $Ro \approx 0.3$, shows an apparent anomaly. For three of the four tests, the Nusselt numbers increase as the Grashof

number increases, but test 4c bucks the trend. This anomaly is believed to be caused by compressibility effects: at high rotational speeds, the temperature of the core increases – and the heat transfer consequently decreases - with radius. For two tests at the same value of Gr but at different values of Re_ϕ , the test at the higher value of Re_ϕ would therefore be expected to produce lower values of the Nusselt numbers.

Inspection of Table 1 shows that, apart from the anomaly referred to above, for each Rossby number the Nusselt numbers increase as the Grashof number increases. However, at a fixed value of the Grashof number, there is a tendency for the Nusselt numbers to decrease as the Rossby number decreases. At small values of Ro (that is, at large values of Re_ϕ), the decrease in Nusselt number can be attributed to compressibility effects. For large values of Ro , where compressibility effects are relatively small, the decrease of Nu_f with decreasing Ro is attributed to the size of the toroidal vortex, which decreases as Ro decreases. As the size of the vortex decreases, the amount of fluid entrained by it decreases, and the temperature of the core would be expected to increase. Consequently, this would decrease the heat transfer from the discs to the core as Ro decreases. More experimental or computational evidence is needed to test this conjecture.

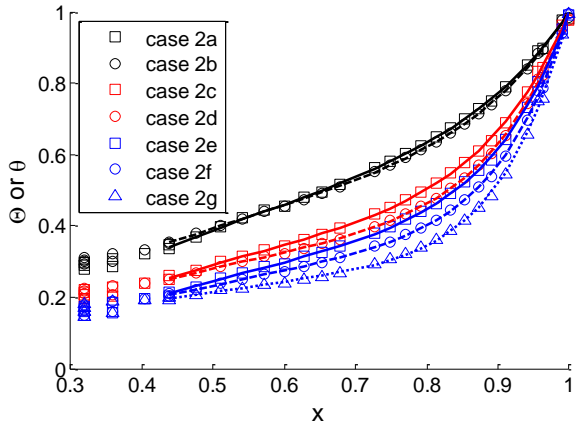


(a) Temperature distributions
(symbols denote measurements; curves show computations)



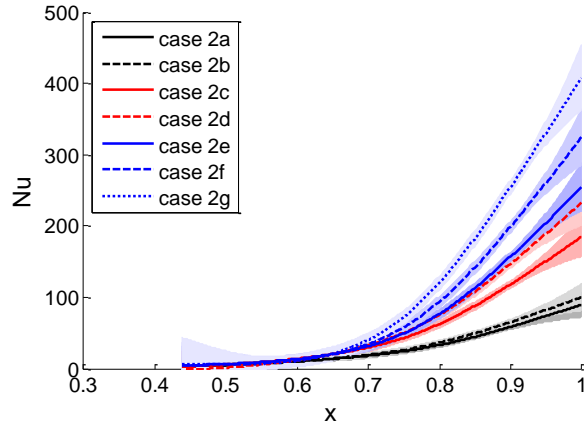
(b) Nusselt number distributions
(curves show computations; shading shows 95% confidence intervals)

Figure 8 Distributions of temperature and Nusselt numbers for $Ro \approx 5$



(a) Temperature distributions

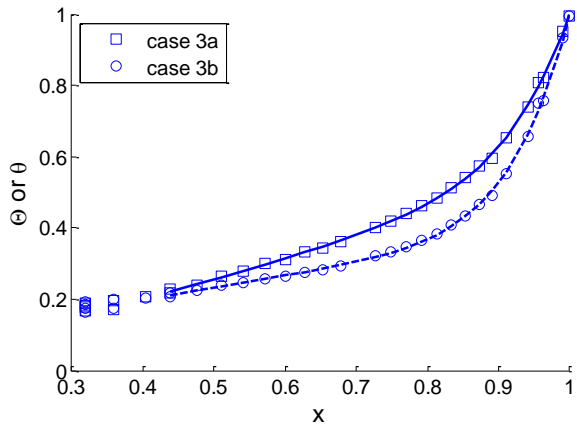
(symbols denote measurements; curves show computations)



(b) Nusselt number distributions

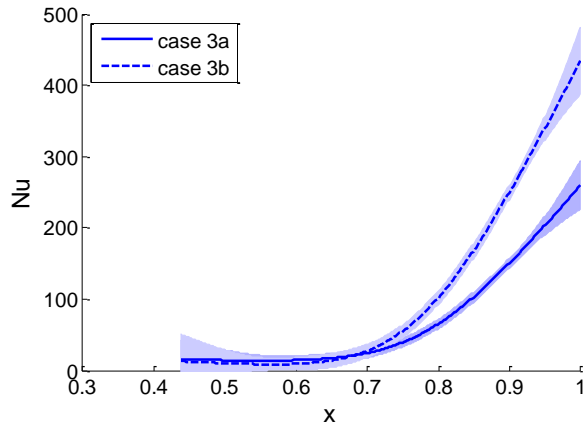
(curves show computations; shading shows 95% confidence intervals)

Figure 9 Distributions of temperature and Nusselt numbers for $Ro \approx 1$



(a) Temperature distributions

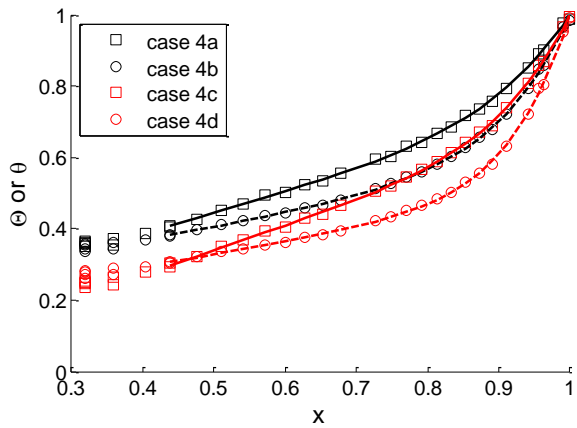
(symbols denote measurements; curves show computations)



(b) Nusselt number distributions

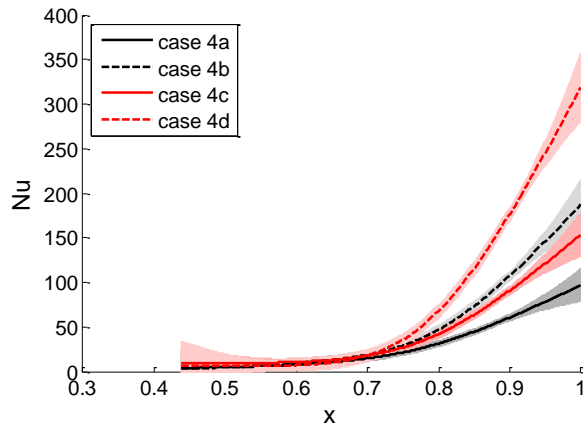
(curves show computations; shading shows 95% confidence intervals)

Figure 10 Distributions of temperature and Nusselt numbers for $Ro \approx 0.6$



(a) Temperature distributions

(symbols denote measurements; curves show computations)



(b) Nusselt number distributions

(curves show computations; shading shows 95% confidence intervals)

Figure 11 Distributions of temperature and Nusselt numbers for $Ro \approx 0.3$

Case No	Ro ≈ 5						Ro ≈ 1						Ro ≈ 0.6		Ro ≈ 0.3				
	1a	1b	1c	1d	1e	1f	2a	2b	2c	2d	2e	2f	2g	3a	3b	4a	4b	4c	4d
<i>Ro</i>	4.7	4.7	4.9	4.9	4.5	4.5	0.8	0.8	0.9	0.9	1.0	1.0	1.0	0.6	0.6	0.3	0.3	0.3	0.3
<i>Gr</i> /10 ¹¹	0.0017	0.003	0.0085	0.015	0.062	0.14	0.065	0.1	0.44	0.84	1.7	2.5	3.9	5.7	9.1	0.4	1.0	3.7	7.8
$\beta\Delta T$	0.08	0.17	0.05	0.11	0.09	0.24	0.09	0.16	0.11	0.23	0.13	0.19	0.32	0.15	0.32	0.06	0.16	0.12	0.29
<i>Re</i> _φ /10 ⁶	0.078	0.077	0.19	0.19	0.46	0.45	0.46	0.45	1.13	1.1	2.1	2.1	2.1	3.5	3.1	1.4	1.4	3.1	3.0
<i>Re</i> _z /10 ⁵	0.19	0.19	0.5	0.5	1.1	1.1	0.19	0.18	0.51	0.5	1.1	1.1	1.1	1.1	1.1	0.2	0.2	0.48	0.48
$\epsilon \times 10^3$	5.2	5.0	4.8	4.4	5.3	5.1	3.9	4.0	5.2	5.8	5.8	6.7	8.1	5.9	8.0	4.5	4.7	4.8	6.6
<i>Nu</i> _b	32.9	38.3	59.3	78.8	141	165	90.0	100	185	233	255	325	408	260	434	97	187	153	318

Table 1 Flow parameters and values of ϵ and Nu_b for experiments of Atkins and Kanjirakkad [16]

6. CONCLUSIONS

A nondimensional form of the fin equation for circular discs has been used to model the heat transfer from air-cooled rotating discs, and Bayesian statistics have been used to determine the Biot numbers, Bi , from the inverse solution of the fin equation. The paper describes how the Bayesian method can be used to determine the values of Bi and their 95% confidence intervals.

The power of the Bayesian method was demonstrated using simulated temperature measurements. First the direct solution of the fin equation was obtained numerically, for the case of a known radial distribution of Bi , and noise was added to the computed disc temperatures to simulate experimental measurements. Next, the Biot numbers were computed, using the ‘experimental temperatures’ as the boundary conditions for the inverse solution of the fin equation. The Bayesian method produced a smooth distribution of Bi , and the computed 95% confidence interval captured the true distribution. By contrast, conventional curve-fitting methods - using polynomials to approximate the experimental temperatures - resulted in large oscillations and inaccurate results.

The Bayesian method was then used to compute the Nusselt numbers, and their confidence intervals, for a compressor disc using published disc-temperature measurements as the boundary conditions for the fin equation. The 19 published test cases covered a wide range of Rossby, rotational Reynolds and Grashof numbers.

For $Ro \approx 5$, $Gr < 3 \times 10^8$ and $Re_\phi < 8 \times 10^4$, where buoyancy effects are expected to be small, the computed values of Nu increased linearly with radius, in a manner consistent with laminar flow over a free disc. For most of the smaller values of Ro and larger values of Gr , where buoyancy effects are expected to be dominant, Nu increased as Gr increased. However, in a few cases at large values of Re_ϕ , where compressibility effects are expected to be significant, two tests at the same value of Gr , but at different values of Re_ϕ , could create different values of Nu : the test at the higher value of Re_ϕ would – as expected - produce the lower value of Nu . Some anomalous behavior at $Ro \approx 0.3$ was attributed to the effect of the toroidal vortex affecting to flow in the cavity.

Although Bayesian statistics have been applied to a number of inverse problems, as far as the authors are aware they have not been

applied to heat transfer from rotating discs. It is hoped that this paper will draw the attention of the research community to the potential use of the methods applied here to other rotating-disc problems.

For heat-transfer experiments on rotating discs, it would be helpful if experimenters were to publish the measured disc temperatures as well as the Nusselt numbers. It should also be remembered that the Nusselt numbers determined from the measured disc temperatures in this paper were an average value for the two surfaces of the disc. In future experiments, if one of the disc surfaces were insulated then the Nusselt numbers could be uniquely assigned to the uninsulated surface. Finally, for any analysis of experimental data, the results can only be as good as the data used to obtain them.

The authors are currently developing a theoretical model of buoyancy-induced flow in rotating cavities, and we shall compare our predictions of the Nusselt numbers with those presented in this paper. We also plan to apply the methods used here to other rotating-disc problems.

ACKNOWLEDGEMENTS

We wish to thank the China Scholarship Council for supporting Hui Tang during her study for a PhD degree at the University of Bath.

APPENDIX

The Bayesian method gives a probability distribution on the Biot numbers rather than a single set of Biot numbers. The MAP estimator is in some sense the most likely profile for the Biot numbers. To give further information about the reliability of the MAP estimator, we show how to find confidence intervals. The confidence intervals that we derive are approximate and depend on a Gaussian approximation to the posteriori distribution, which is effective when the posterior variance is small (i.e. the data can be well approximated).

Recall from eq (23) that the posterior potential

$$F(Bi|\theta) = (M) \ln \epsilon + \frac{(\theta - \theta(Bi))^T (\theta - \theta(Bi))}{2\epsilon^2} + \frac{1}{2} Bi^T C^{-1} Bi \quad (A1)$$

where θ is the vector containing the experimental data points $\theta_j (j \in J_\theta)$ and θ is a vector containing the corresponding $\theta_j (j \in J_\theta)$. Denote the MAP estimator by Bi_0 and compute the Taylor expansion of the posterior potential around Bi_0 :

$$F(Bi|\theta) = F + \frac{\partial F}{\partial Bi}(Bi - Bi_0) + \frac{1}{2}(Bi - Bi_0)^T \frac{\partial^2 F}{\partial Bi^2}(Bi - Bi_0) + \text{higher order terms} \quad (\text{A2})$$

where all the F terms on the right-hand side are evaluated at Bi_0 . If $Bi - Bi_0$ is small, the higher-order terms can be dropped. It is the second-order terms that define the covariance of the approximating Gaussian distribution and that determine the confidence intervals. This method is known as the Laplace approximation.

As Bi_0 is the MAP estimator, it minimises F and the first-order necessary condition is

$$\frac{\partial F}{\partial Bi} |_{Bi=Bi_0} = 0 \quad (\text{A3})$$

The second derivative of F is

$$\frac{\partial^2 F}{\partial Bi^2} = \frac{1}{2\epsilon^2} \frac{\partial^2}{\partial Bi^2} (\theta - \theta)^T (\theta - \theta) + \frac{1}{2} \frac{\partial^2}{\partial Bi^2} Bi^T C^{-1} Bi \quad (\text{A4})$$

Note that

$$\frac{\partial^2 (\theta - \theta)^T (\theta - \theta)}{\partial Bi^2} = 2J^T J - 2(\theta - \theta)^T \frac{\partial^2 \theta}{\partial Bi^2} \quad (\text{A5})$$

where the Jacobian matrix $J = \partial \theta / \partial Bi$. The finite-difference method for the fin eq.(17) can be written

$$E(Bi)\theta = d \quad (\text{A6})$$

where d is the fixed vector from the fin eq. (17). Note that the θ here only contain the corresponding θ_j where $j \in J_\theta$. The product rule for differentiation gives

$$\frac{\partial E}{\partial Bi_j} \theta + E \frac{\partial \theta}{\partial Bi_j} = 0 \quad (\text{A7})$$

hence

$$\frac{\partial \theta}{\partial Bi_j} = -E^{-1} \frac{\partial E}{\partial Bi_j} \theta \quad (\text{A8})$$

The vectors $\partial \theta / \partial Bi_j$ gives the columns of the J . In eq.(A5), we assume that $\theta - \theta$ is small and, as the experimental data is well approximated by the model, we neglect the last term in the equation. Then, substitute into eq. (A4), to find

$$\frac{\partial^2 F}{\partial Bi^2} \approx \frac{J^T J}{\epsilon^2} + C^{-1} \quad (\text{A9})$$

Eqs (A9) and (A2) give

$$F(Bi|\theta) \approx F(Bi_0|\theta) + \frac{1}{2}(Bi - Bi_0)^T Q (Bi - Bi_0) \quad (\text{A10})$$

The posterior distribution has the density function proportional to $\exp(-F(Bi|\theta))$. This gives a new distribution with probability density function proportional to $\exp(-\frac{1}{2}(Bi - Bi_0)^T Q (Bi - Bi_0))$, which is a mean-zero multivariate Gaussian distribution with covariance

$$Q^{-1} = \left(\frac{J^T J}{\epsilon^2} + C^{-1} \right)^{-1} \quad (\text{A11})$$

We use this distribution to determine confidence intervals. Let σ_{Bi_j} denote the square root of the j^{th} element on the leading diagonal of the covariance matrix. Then the 95% confidence intervals for each Bi are taken to be

$$Bi_{0,j} \pm 1.96\sigma_{Bi_j} \quad (\text{A12})$$

REFERENCES

1. Incropera, F. P., and DeWitt, D. P., 1996. Fundamentals of heat and mass transfer. Wiley, New York.
2. Kaipio, J., and Somersalo E., 2005. Statistical and computational inverse problems. Vol. 160. Springer, New York.
3. Kaipio, J. P., and Fox, C., 2011. The Bayesian framework for inverse problems in heat transfer. Heat Trans. Eng., 32(9), 718-753.
4. Orlande, H. R., 2012. Inverse problems in heat transfer: new trends on solution methodologies and applications. ASME J. Heat Transfer, 134(3), 031011.
5. Wang, J., and Zabarar, N., 2004. A Bayesian inference approach to the inverse heat conduction problem. Int. J. Heat Mass Trans., 47(17), 3927-3941.
6. Gnanasekaran, N., and Balaji, C., 2011. A Bayesian approach for the simultaneous estimation of surface heat transfer coefficient and thermal conductivity from steady state experiments on fins. Int. J. Heat Mass Trans. 54(13), 3060-3068.
7. Owen, J. M., Long, C. A., 2015. Review of buoyancy-induced flow in rotating cavities. ASME J. Turbomach. Accepted for publication.
8. Childs, P. R., 2010. Rotating flow. Elsevier, Oxford.
9. Owen, J. M., and Rogers, R. H., 1995. Flow and heat transfer in rotating disc systems, Vol. 2: Rotating Cavities. Research Studies Press, Taunton. (John Wiley, New York.)

10. Tritton, D. J., 1988. Physical fluid dynamics. Oxford, Clarendon Press, Oxford.
11. Owen, J. M., and Pincombe, J.R., 1979. Vortex breakdown in a rotating cylindrical cavity. *J. Fluid Mech.*, 90(01), 109-127.
12. Farthing, P.R., Long, C.A., Owen, J.M. and Pincombe, J.R. 1992. Rotating cavity with axial throughflow of cooling air: flow structure. *ASME J. Turbomach.*, 114, pp. 237-246.
13. Farthing, P.R., Long, C.A., Owen, J.M. and Pincombe, J.R. 1992. Rotating cavity with axial throughflow of cooling air: heat transfer. *ASME J. Turbomach.*, 114, pp. 229-236.
14. Bohn, D. E., Deutsch, G. N., Simon, B., and Burkhardt, C., 2000. Flow visualisation in a rotating cavity with axial throughflow. *ASME Paper 2000-GT-280*.
15. Long, C. A., and Childs, P. R. N., 2007. Shroud heat transfer measurements inside a heated multiple rotating cavity with axial throughflow. *Int.J. Heat Fluid Flow*, 28(6), 1405-1417.
16. Atkins, N. R., and Kanjirakkad, V., 2014. Flow in a Rotating Cavity With Axial Throughflow at Engine Representative Conditions. *ASME Paper GT2014-27174*.
17. Matérn, B., 1960. Spatial variation. Stochastic models and their application to some problems in forest surveys and other sampling investigations. *Meddelanden fran statens Skogsforskningsinstitut*, 49(5).
18. Stein, M. L. 1999. *Interpolation of Spatial Data: Some Theory for Kriging*. Springer, New York.
19. Tikhonov, A.N., 1977. *Solution of ill-posed problems*. Halsted Press, Washington.
20. Chorin, A. J., and Hald, O. H., 2009. *Stochastic tools in mathematics and science*(Vol. 1). Dordrecht: Springer.
21. Alexiou, A., Hills, N. J., Long, C. A., Turner, A. B., and Millward, J. A., 2000. Heat transfer in high-pressure compressor gas turbine internal air systems: A rotating disc-cone cavity with axial throughflow. *Exp. Heat Trans.*, 13(4), 299-328.
22. Miché, N. D., 2009. *Flow and heat transfer measurements inside a heated multiple rotating cavity with axial throughflow* . DPhil., University of Sussex, UK.
23. Günther, A., Uffrecht, W., and Odenbach, S., 2012. Local measurements of disk heat transfer in heated rotating cavities for several flow regimes. *ASME J. Turbomach.*, 134(5), 051016.
24. Günther, A., Uffrecht, W., & Odenbach, S., 2014. The effects of rotation and mass flow on local heat transfer in rotating cavities with axial throughflow. *ASME Paper GT2014-26228*
25. Owen, J.M. and Rogers, R.H., 1989. *Flow and heat transfer in rotating-disc systems, Vol.1: Rotor-stator systems*. Research Studies Press, Taunton. (John Wiley, New York.)